

Supporting Information

Finely tuned framework isomers for highly efficient C₂H₂ and CO₂ separation

Shuang Liu,^{†,‡,§} Yuhang Huang,^{†,§} Qiubing Dong,[†] Huijie Wang[†] and Jingui Duan^{†*}

[†]State Key Laboratory of Materials-Oriented Chemical Engineering, College of Chemical Engineering, Nanjing Tech University, Nanjing 211816, China

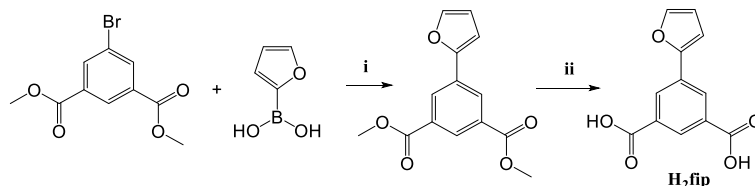
[‡]School of Chemistry & Chemical Engineering, Shangqiu Normal University, Shangqiu 476000, China

1. Materials and methods

All reagents and solvents were commercially available and used as received. The elemental analysis was carried out with a Perkin-Elmer 240C elemental analyzer. The Fourier-transform Infrared (FT-IR) spectra were recorded from KBr pellets in the range of 4000–600 cm^{-1} on a VECTOR 22 spectrometer. Thermogravimetric analyses (TGA) were performed using a STA 209 F1 (NETZSCH Instruments) thermo-microbalance, heating from room temperature to 600°C at a rate of 10°C min^{-1} under nitrogen flow. Simulated powder patterns from single-crystal X-ray diffraction data were generated using Mercury 1.4.2 software. ^1H NMR spectra were recorded on a Bruker Advance III 600 MHz NMR Spectrometer. The coincident XRPD/adsorption measurements were performed with a Rigaku Ultima IV with $\text{CuK}\alpha$ radiation connected to a BELSORP-18PLUS volumetric adsorption setup (Bel Japan, Inc.). The respective apparatuses were synchronized to enable each PXRD pattern to be obtained at each equilibrium point of the sorption isotherms.

2. Ligand synthesis

The ligand of 5-(furan-2-yl)isophthalic acid (**H₂fip**) was synthesized by Suzuki coupling reaction in high overall yield, shown in Scheme S1.¹



Scheme S1. Synthesis of **H₂fip**: i) K₂CO₃, Pd(PPh₃)₄, C₆H₅CH₃/MeOH/H₂O, 90°C, 48 h, 70.0%.
ii) NaOH, THF/MeOH, reflux 16 h, then 3M HCl_(aq), 95.2%.

Synthesis of dimethyl 5-(furan-2-yl)isophthalate

After adding the mixture of dimethyl 5-bromoisophthalate (2.73 g, 10 mmol) and furan-2-ylboronic acid (1.34 g, 12 mmol), Pd(PPh₃)₄ (450 mg, 0.4 mmol) and K₂CO₃ (2.76 g, 20 mmol) into toluene/methanol/water (125/30/30 mL), the solution was bubbled by N₂ for 30 min. The mixture was stirred at 90°C for 48 h under N₂ atmosphere. The organic solvents were removed and the residue was extracted with CH₂Cl₂ (3 × 70 mL), the organics washed with water (2 × 20 mL), dried with MgSO₄, filtered and concentrated. The residue was purified by column chromatography (silica gel, EtOAc/Petroleum ether) to afford white solid of **C** (1.96 g, 70.0%). ¹H NMR (600 MHz, DMSO-d₆): δ 8.555 (s, 1H), 8.505 (s, 2H), 7.533 (s 1H), 6.827 (t, 1H), 6.523 (t, 1H), 3.979 (s, 6H) (Fig. S1).

Synthesis of 5-(furan-2-yl)isophthalic acid (**H₂fip**)

C (1 g, 3.62 mmol) and NaOH (2.9 g, 72.5 mmol) were added to a solution of THF/MeOH/H₂O (36/36/72 mL). Then, the solution was heated at reflux for 16 hours. After the temperature cooling down, the reaction mixture was evaporated to dryness and the residue dissolved in water and filtered. The filtrate was acidified to pH = 3 with 3M HCl and the resulting precipitate collected, washed thoroughly with water and dried to afford **H₂fip** (0.79 g, 95.2%) as an off-white powder. ¹H NMR (600 MHz, DMSO-d₆): δ = 13.477 (s, 2H), 8.43 (s, 2H), 8.40 (s, 1H), 8.35 (s, 2H), 7.70 (d, 1H), 7.66 (d, 1H), 7.19 (t, 1H) (Fig. S2).

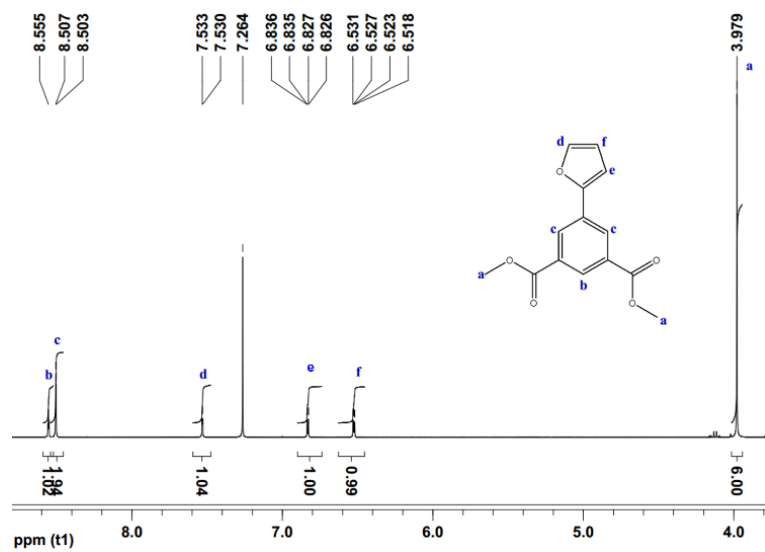


Figure S1. ¹H NMR spectrum of dimethyl 5-(furan-2-yl)isophthalate (C).

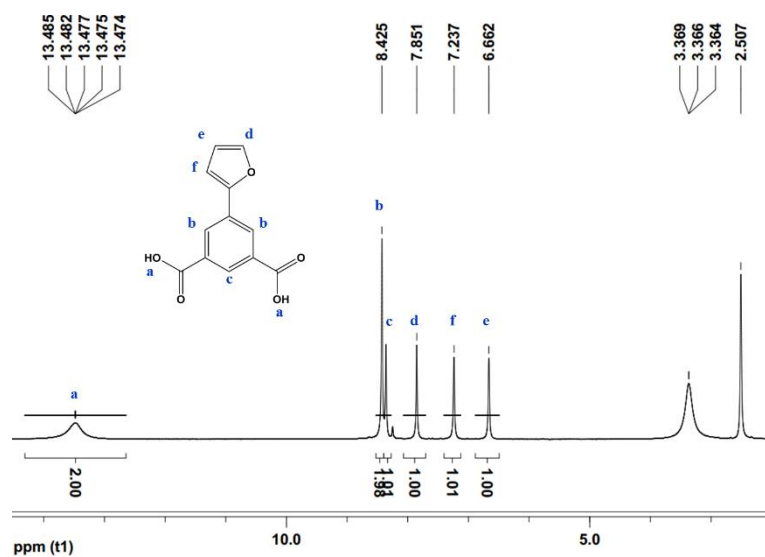


Figure S2. ¹H NMR spectrum of 5-(furan-2-yl)isophthalic acid (H₂fip).

3. Crystallographic analysis

Single-crystal X-ray diffraction measurements were performed on a Bruker Smart Apex CCD diffractometer at 298 K using graphite monochromated Mo/K α radiation ($\lambda = 0.71073 \text{ \AA}$). Data reduction was made with the Bruker Saint program. The structures were solved by direct methods and refined with full-matrix least squares technique using the SHELXTL package². Non-hydrogen atoms were refined with anisotropic displacement parameters during the final cycles. Organic hydrogen atoms were placed in calculated positions with isotropic displacement parameters set to $1.2 \times U_{eq}$ of the attached atom. The hydrogen atoms of the ligand and water molecules could not be located, but are included in the formula. The unit cell includes a region of disordered solvent molecules, which could not be modeled as discrete atomic sites. We employed PLATON/SQUEEZE^{3, 4} to calculate the diffraction contribution of the solvent molecules and, thereby, to produce a set of solvent-free diffraction intensities; structures were then refined again using the data generated. CCDC 1974514-1974517 contains the supplementary crystallographic data for this paper. These data can be obtained free of charge from The Cambridge Crystallographic Data Centre via www.ccdc.cam.ac.uk/data_request/cif. Crystal data are summarized in Table S1.

Table S1. Crystal data and structure refinement of the four PCP structures.

Name	NTU-51	NTU-52	NTU-53	NTU-54
Empirical formula	C ₁₂ H ₈ CuO ₆	C ₁₂ H ₈ CuO ₆	C ₁₂ H ₈ CuO ₆	C ₁₂ H ₈ CuO ₆
Formula weight	311.73	311.73	311.73	311.73
Space group	<i>P4/nmm</i>	<i>I4₁22</i>	<i>R-3</i>	<i>P-3m1</i>
<i>a</i> / Å	19.081(4)	10.605(7)	18.3147(12)	18.675(2)
<i>b</i> / Å	19.081(4)	10.605(7)	18.3147(12)	18.675(2)
<i>c</i> / Å	10.235(2)	30.82(4)	22.670(3)	6.9982(11)
$\alpha = \beta$ / °	90	90	90	90
γ / °	90	90	120	120
<i>V</i> / Å ³	3726.4(17)	3466(6)	6585.4(14)	2113.7(6)
<i>Z</i>	8	8	18	6
<i>D</i> _{calc} / gcm ⁻³	1.111	1.195	1.415	1.413
μ / mm ⁻¹	1.185	1.274	1.508	1.563
Θ range°	1.5, 25.0	2.0, 25.1	1.6, 25.1	1.3, 25.1
Index ranges	-22 ≤ <i>h</i> ≤ 22 -22 ≤ <i>k</i> ≤ 22 -11 ≤ <i>l</i> ≤ 12	-10 ≤ <i>h</i> ≤ 12 -12 ≤ <i>k</i> ≤ 12 -36 ≤ <i>l</i> ≤ 36	-21 ≤ <i>h</i> ≤ 21 -20 ≤ <i>k</i> ≤ 21 -26 ≤ <i>l</i> ≤ 27	-22 ≤ <i>h</i> ≤ 22 -21 ≤ <i>k</i> ≤ 22 -8 ≤ <i>l</i> ≤ 8
<i>R</i> ₁	0.1181	0.0725	0.0568	0.0627
<i>wR</i> _{2a} [<i>I</i> > 2σ(<i>I</i>)]	0.3480	0.2016	0.1791	0.1784
GOF	1.040	1.057	1.090	1.10

$$R_1 = \sum ||F_o| - |F_c|| / \sum |F_o|; wR_2 = [\sum w(\sum F_o^2 - F_c^2)^2 / \sum w(F_o^2)^2]^{1/2}$$

4. Crystal structural details

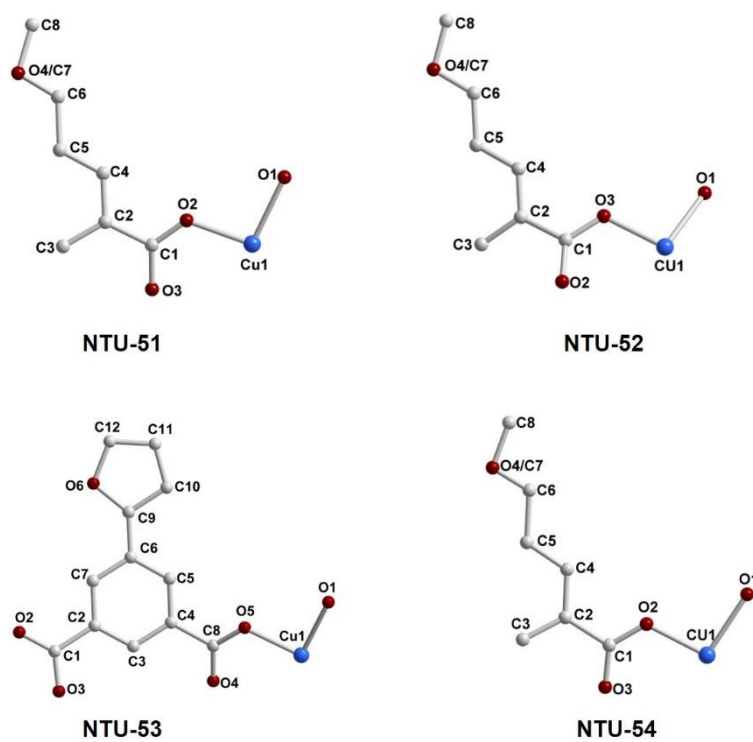


Figure S3. Asymmetric unit of NTU-51 to NTU-54.

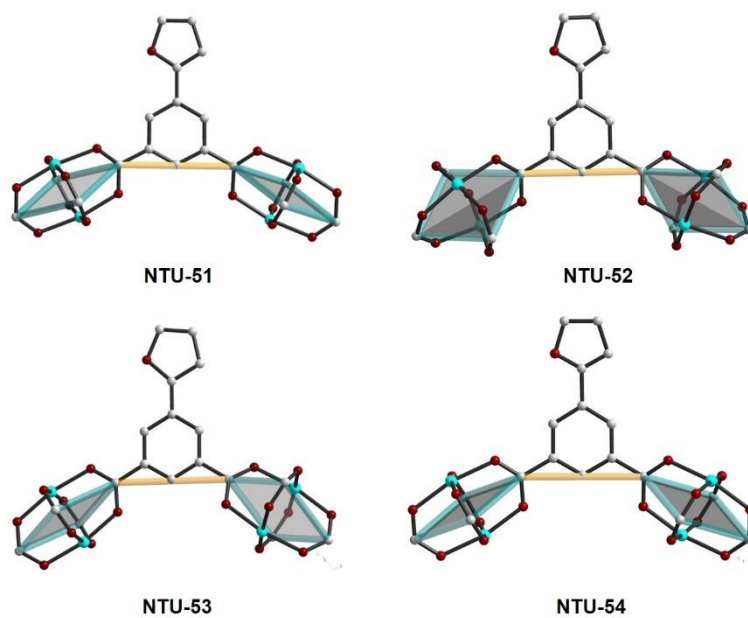


Figure S4. Ligand connection in NTU-51 to NTU-54. Each ligand was bridged by two Cu paddlewheel clusters.

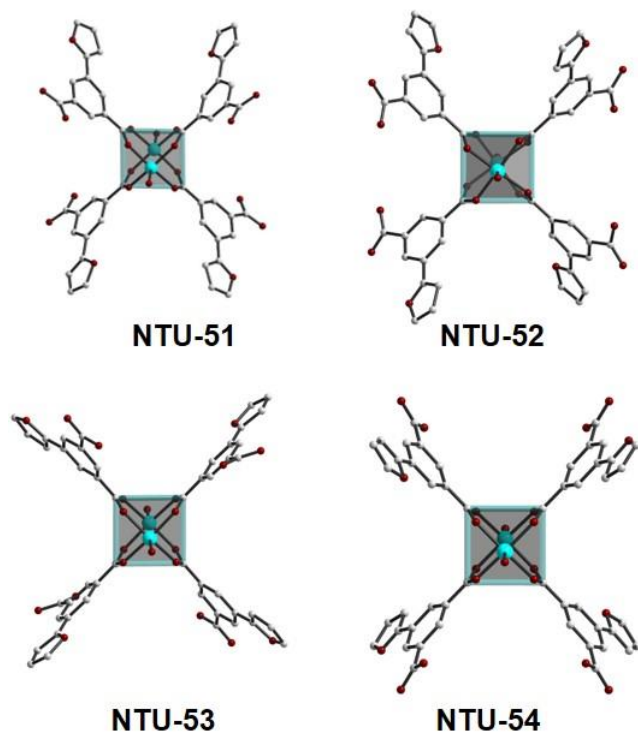


Figure S5. Cluster connection in NTU-51 to NTU-54. Each cluster was bridged by four ligands.

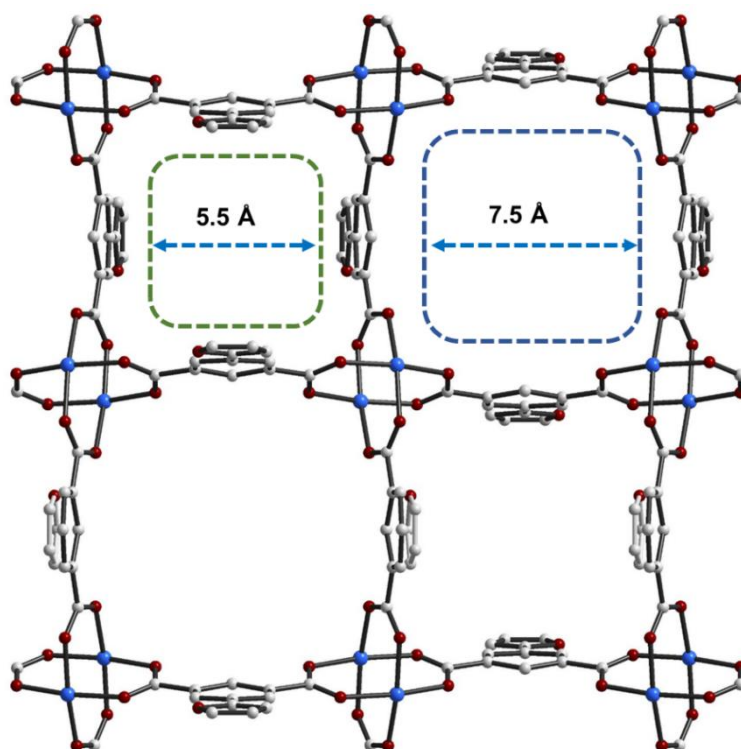


Figure S6 View of the pores in the 2D framework of NTU-51.

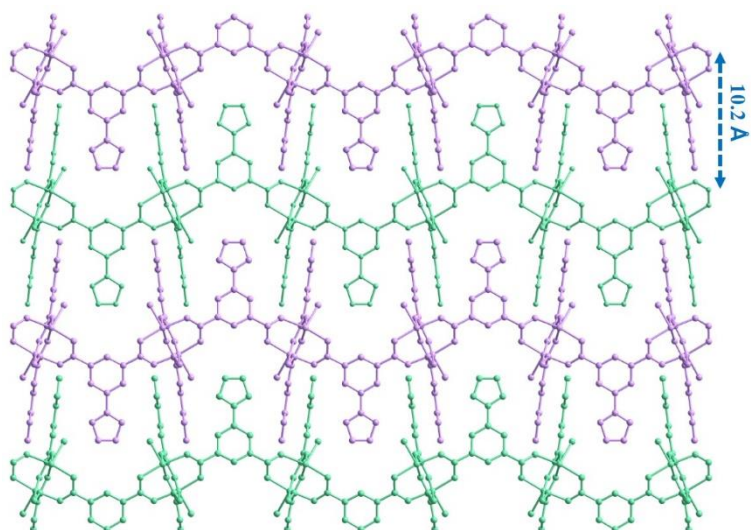


Figure S7. Packing view of NTU-51. The layer distance is 10.2 Å.

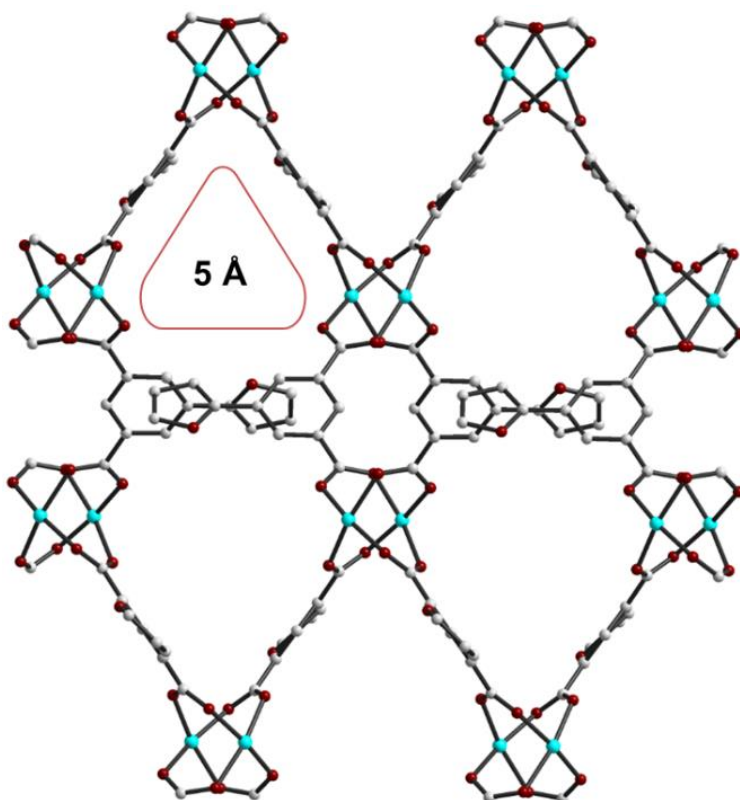


Figure S8. View of tailored pore in NTU-52.

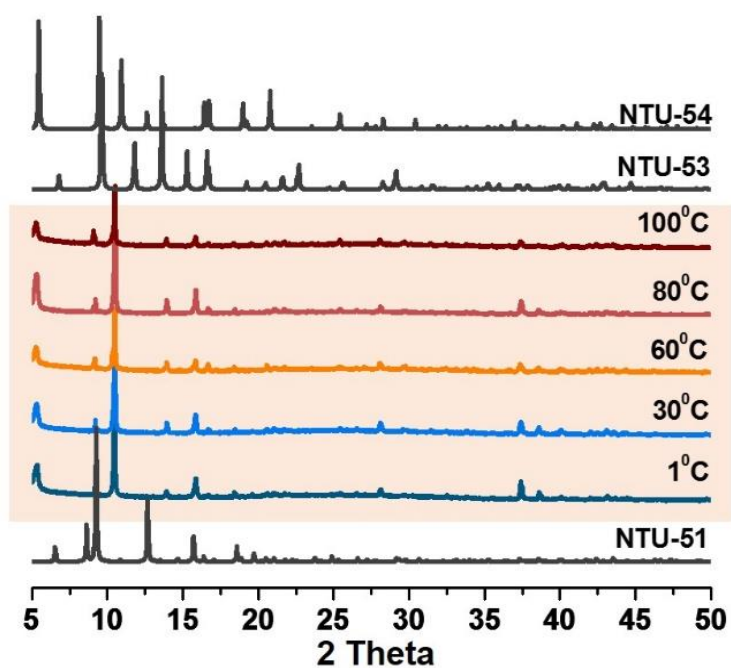


Figure S9. PXRD of NTU-51 after water treatment at different temperatures for 2 weeks (1, 30, 60 and 80°C).

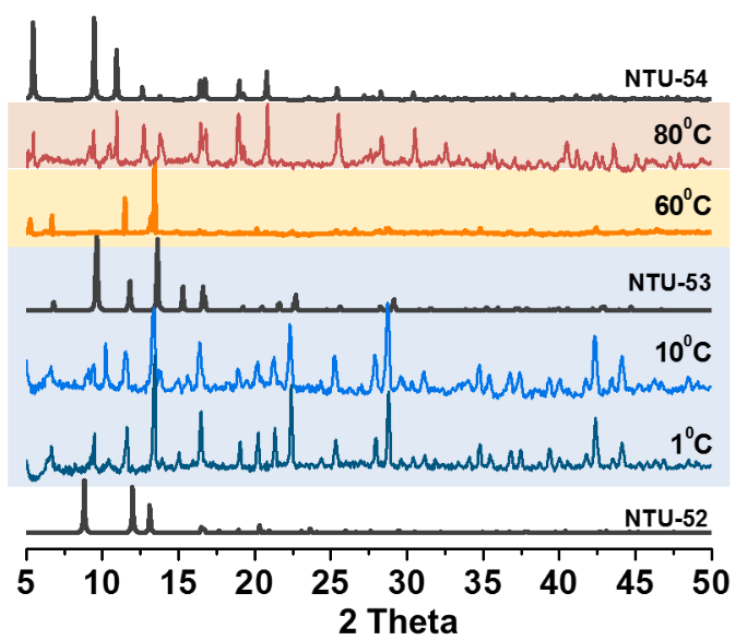


Figure S10. PXRD of NTU-52 after water treatment at different temperatures for 2 weeks (1, 10, 60 and 80°C).

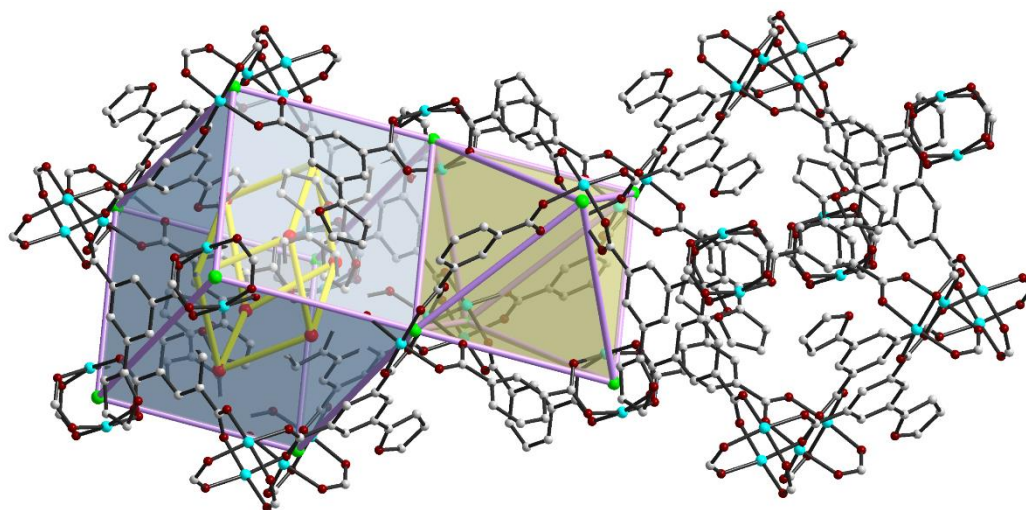


Figure S11. Two kind of cages in NTU-53. The one features double layered structure.

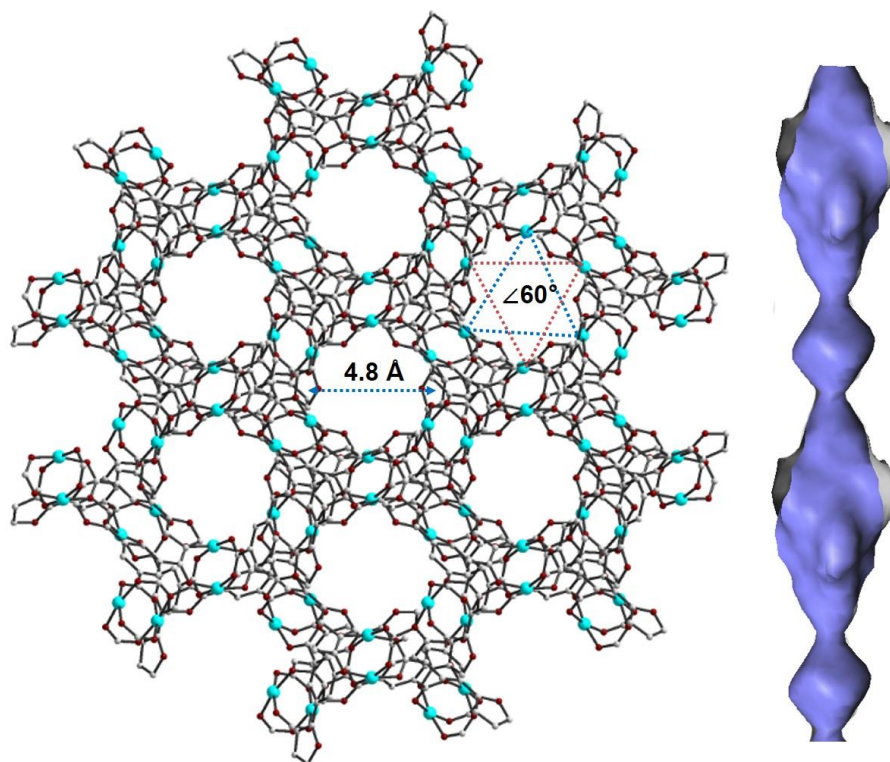


Figure S12. Packing view of NTU-53 along *c*-axis (left), in which a kind of 1D channel with window aperture of 4.8 Å was found.

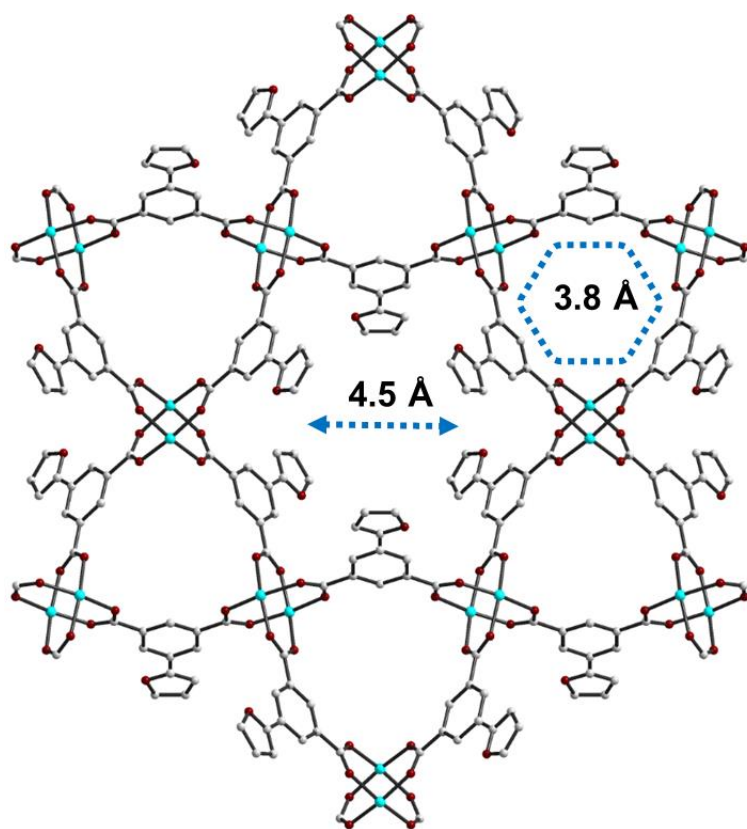


Figure S13. View of two pores in NTU-54 along *c*-axis.

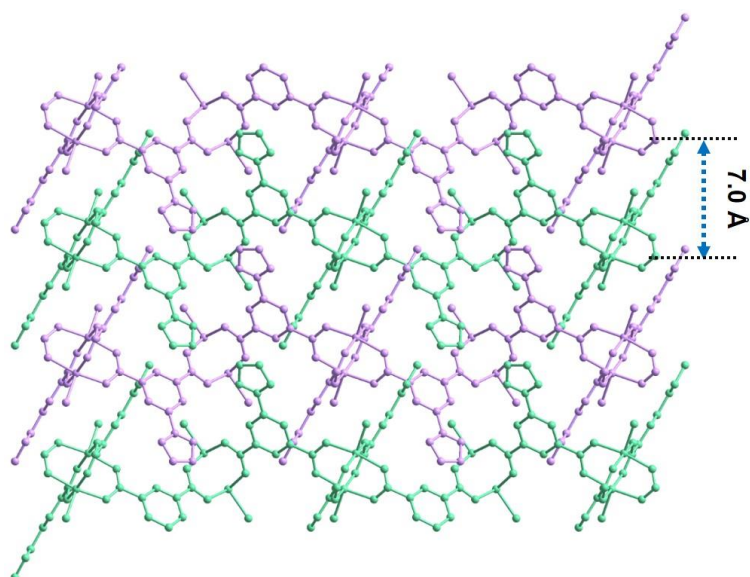


Figure S14. Stacked layers of NTU-54. The layer distance is 7.0 Å.

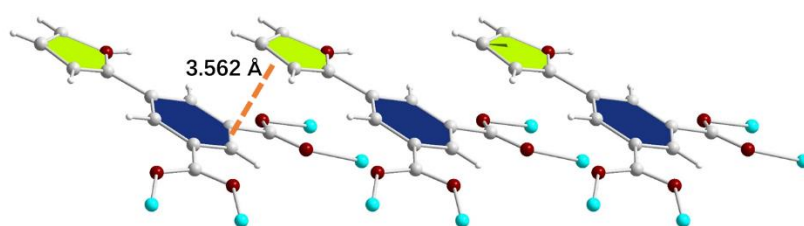


Figure S15. View of face-to-face packed furan and benzene rings in NTU-54.

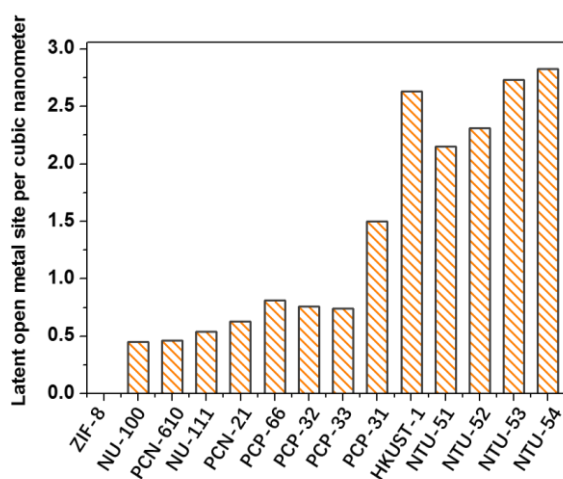


Figure S16. Calculated number of latent open metal site per cubic nanometer in series PCPs. Note: The values in this figure are calculated from the information of the reported *.cif (HKUST-1⁵, PCN-21⁶, NU-111⁷, ZIF-8⁸, PCN-66⁹, NU-100¹⁰, PCN-610¹¹, PCP-31¹², PCP-32¹², PCP-33¹³), and also the *.cif in this work.

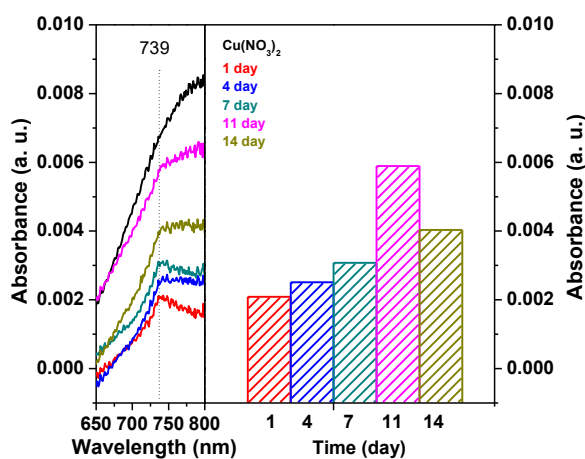


Figure S17. In-situ UV/Vis spectra of the crystal transformation from NTU-52 to NTU-53. The bar graph to the right of the spectra details the increase in absorption at 739 nm.

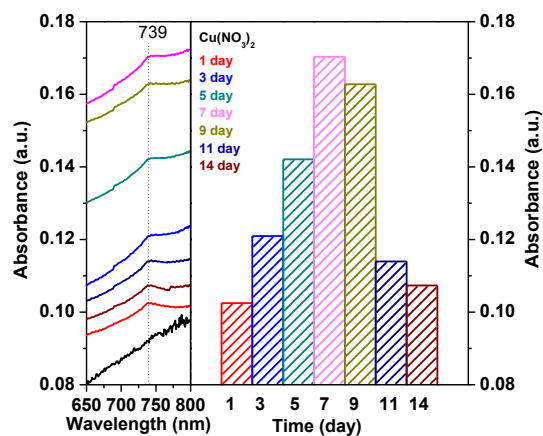


Figure S18. In-situ UV/Vis spectra of the crystal transformation from NTU-52 to NTU-54. The bar graph to the right of the spectra details the increase in absorption at 739 nm.

5. Characterization

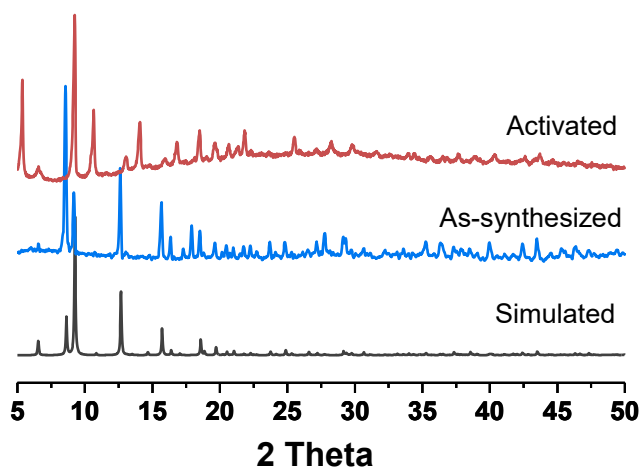


Figure S19. PXRD of three phases of NTU-51. The activated phase showed shift of the X-ray diffraction, indicating the changed 2D structure.

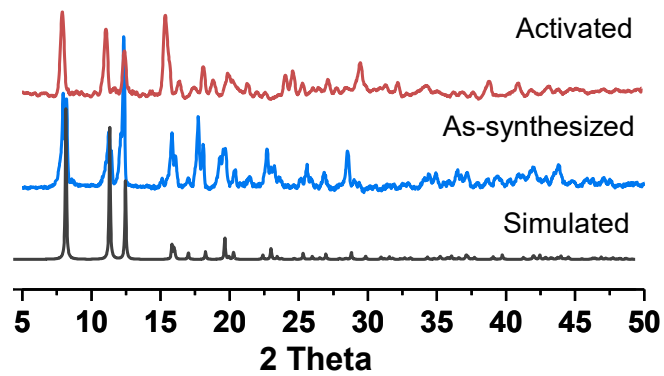


Figure S20. PXRD of three phases of NTU-52.

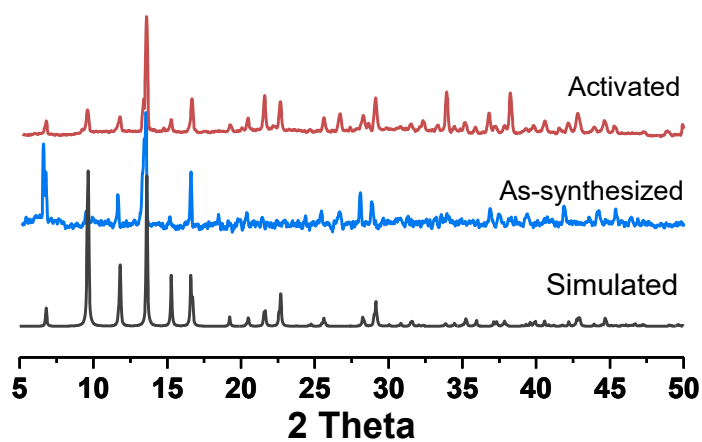


Figure S21. PXRD of three phases of NTU-53.

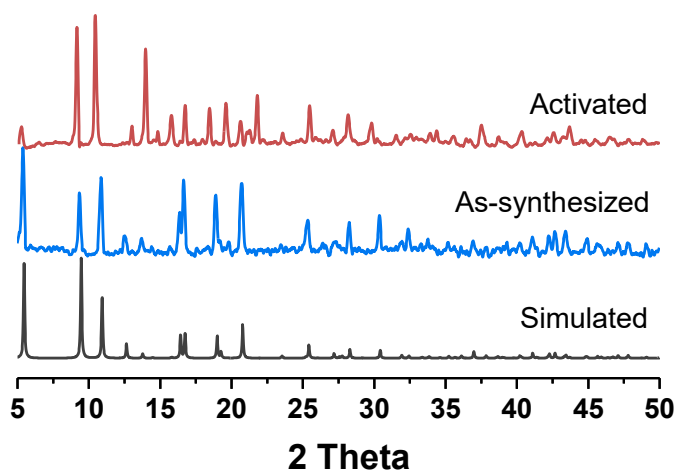


Figure S22. PXRD of three phases of NTU-54.

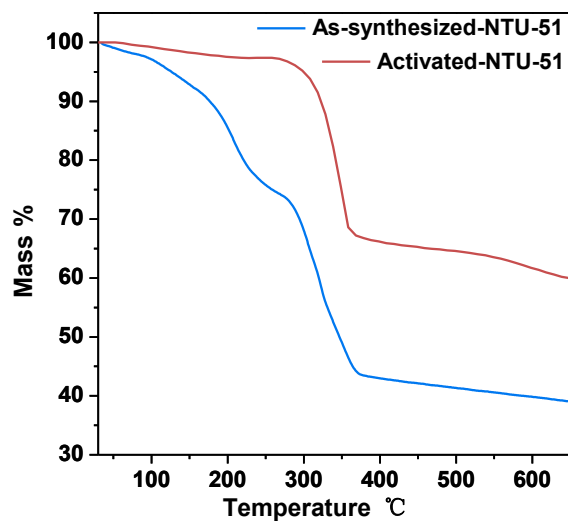


Figure S23. TG curves of NTU-51.

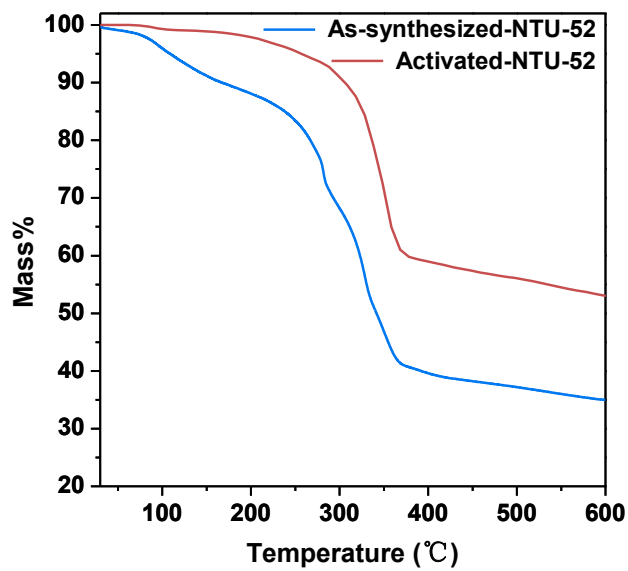


Figure S24. TG curves of NTU-52.

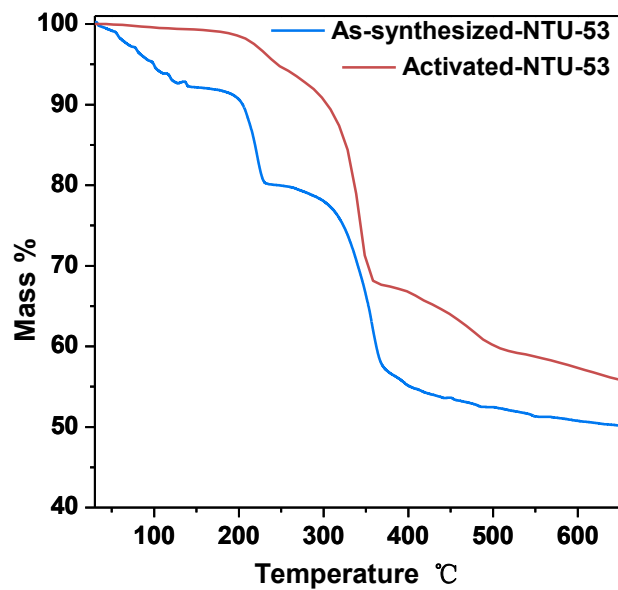


Figure S25. TG curves of NTU-53.

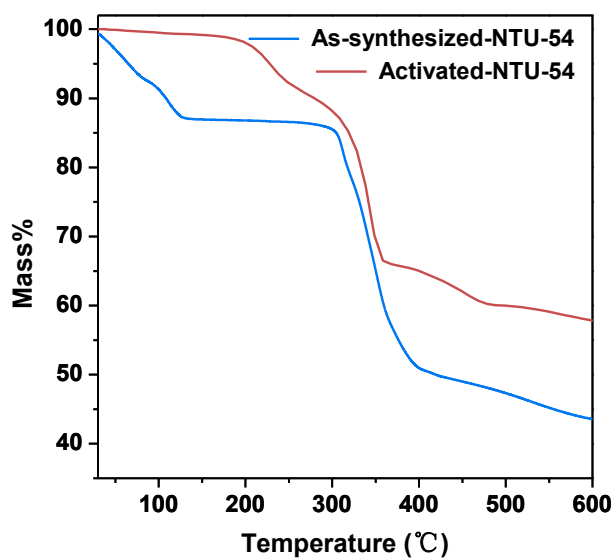


Figure S26. TG curves of NTU-54.

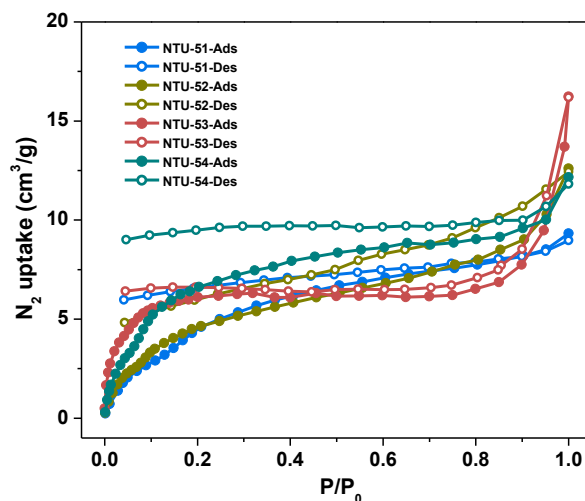


Figure S27. N_2 adsorption of NTU-51 to NTU-54 at 77K. Ads and Des are abbreviation of adsorption and desorption, respectively.

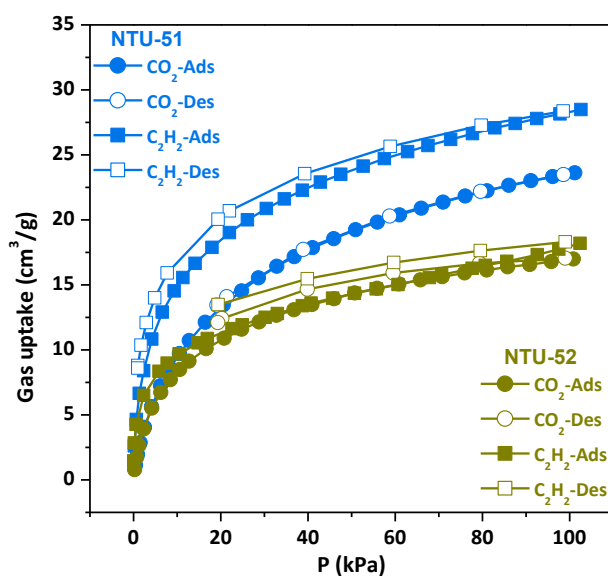


Figure S28. Low pressure C_2H_2 and CO_2 adsorption and desorption isotherms of NTU-51 and NTU-52 at 273 K.

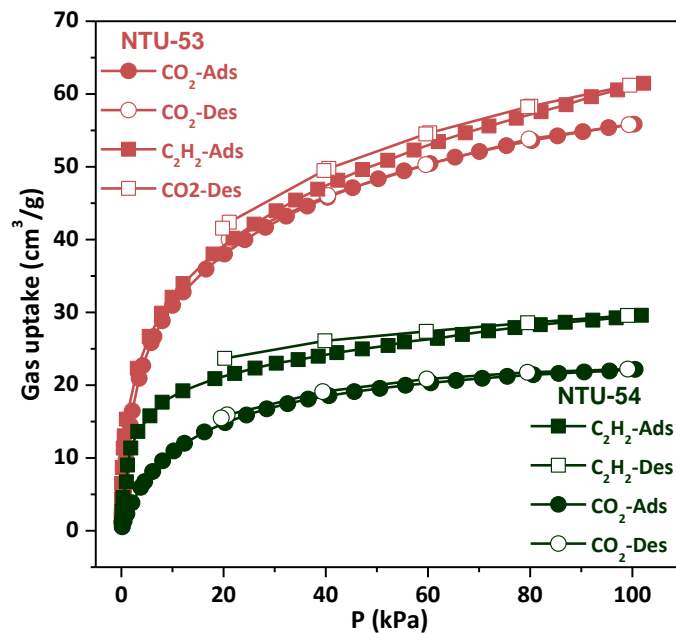


Figure S29. Low pressure C_2H_2 and CO_2 adsorption and desorption isotherms of NTU-53 and NTU-54 at 273 K.

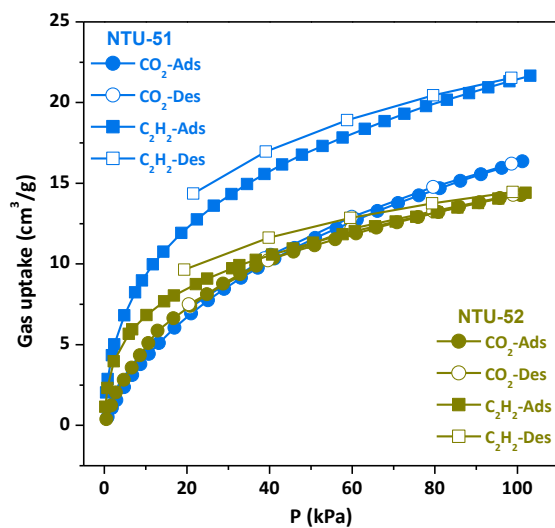


Figure S30. Low pressure C_2H_2 and CO_2 adsorption and desorption isotherms of NTU-51 and NTU-52 at 298 K.

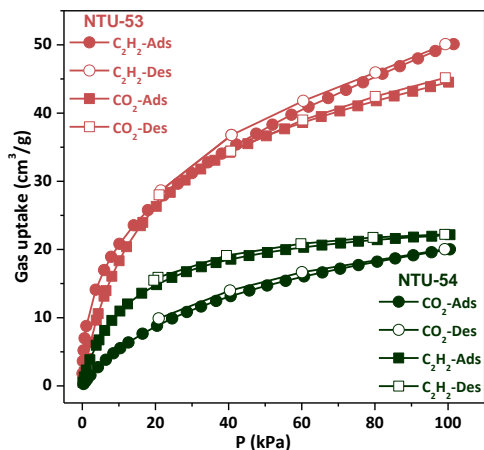


Figure S31. Low pressure C_2H_2 and CO_2 adsorption and desorption isotherms of NTU-53 and NTU-54 at 298 K.

6. Estimation of the isosteric heats of gas adsorption

A virial-type expression comprising the temperature-independent parameters a_i and b_i was employed to calculate the enthalpies of adsorption for C_2H_2 and CO_2 . In each case, the data were fitted using the equation:

$$\ln P = \ln N + 1/T \sum_{i=0}^m a_i N^i + \sum_{i=0}^n b_i N^i \quad (1)$$

Here, P is the pressure expressed in Torr, N is the amount adsorbed in mmol/g, T is the temperature in K, a_i and b_i are virial coefficients, and m , n represent the number of coefficients required to adequately describe the isotherms (m and n were gradually increased until the contribution of extra added a and b coefficients was deemed to be statistically insignificant towards the overall fit, and the average value of the squared deviations from the experimental values was minimized).

$$Q_{st} = -R \sum_{i=0}^m a_i N^i \quad (2)$$

Here, Q_{st} is the coverage-dependent isosteric heat of adsorption and R is the universal gas constant.

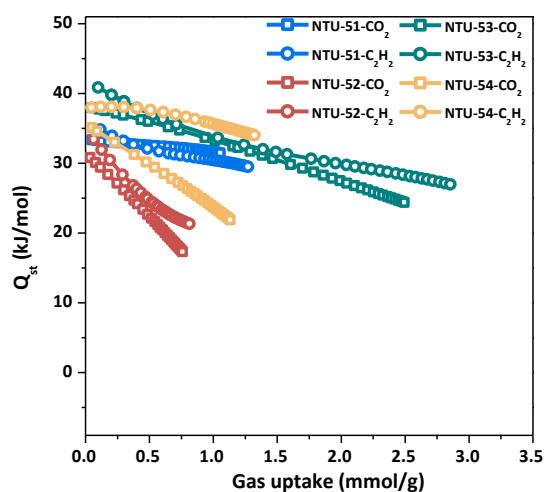


Figure S32. The calculated adsorption heats of NTU-51 to NTU-54.

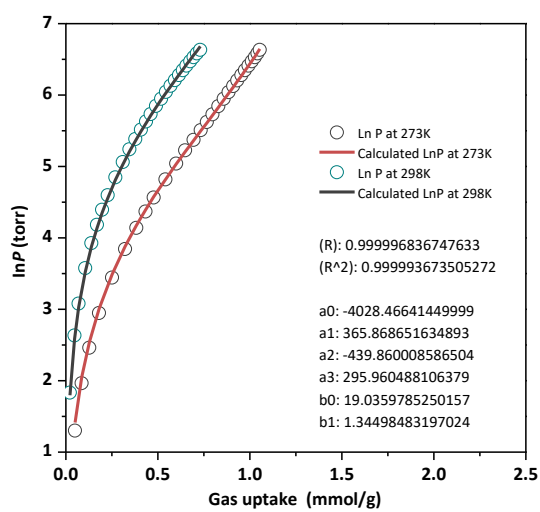


Figure S33. The calculated virial equation isotherms parameters fit to the experimental CO₂ data (at 273 and 298K) of NTU-51.

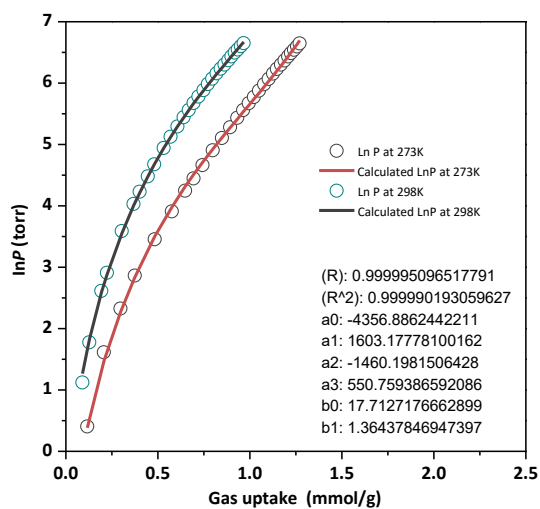


Figure S34. The calculated virial equation isotherms parameters fit to the experimental C_2H_2 data (at 273 and 298K) of NTU-51.

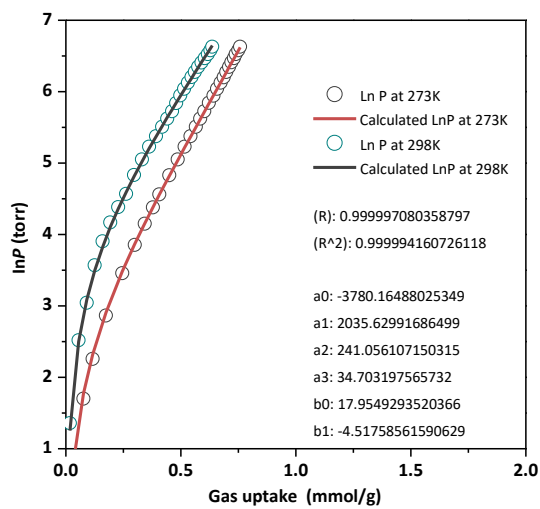


Figure S35. The calculated virial equation isotherms parameters fit to the experimental CO_2 data (at 273 and 298K) of NTU-52.

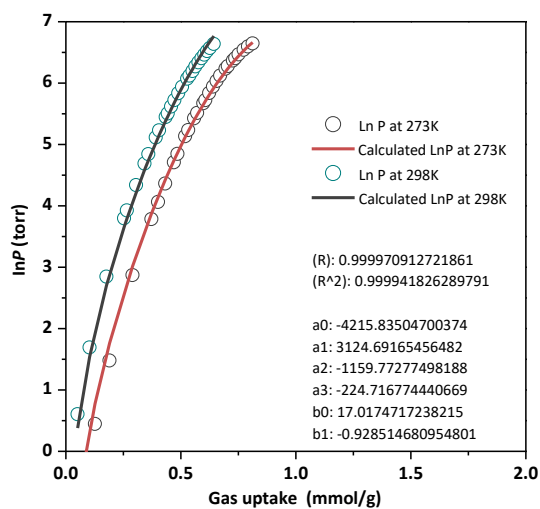


Figure S36. The calculated virial equation isotherms parameters fit to the experimental C₂H₂ data (at 273 and 298K) of NTU-52.

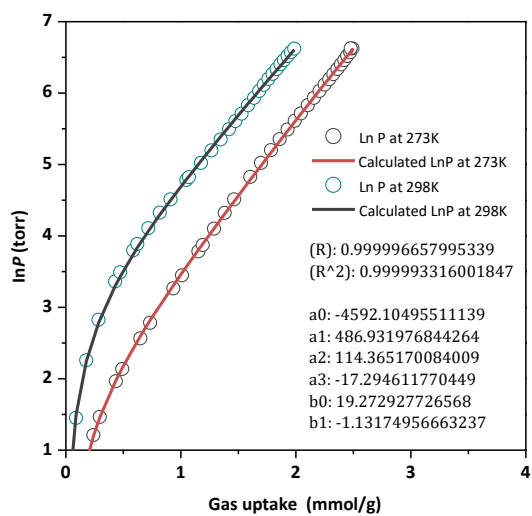


Figure S37. The calculated virial equation isotherms parameters fit to the experimental CO₂ data (at 273 and 298K) of NTU-53.

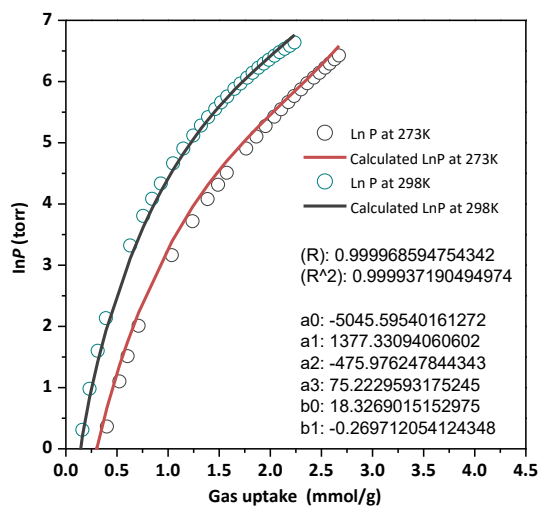


Figure S38. The calculated virial equation isotherms parameters fit to the experimental C_2H_2 data (at 273 and 298K) of NTU-53.

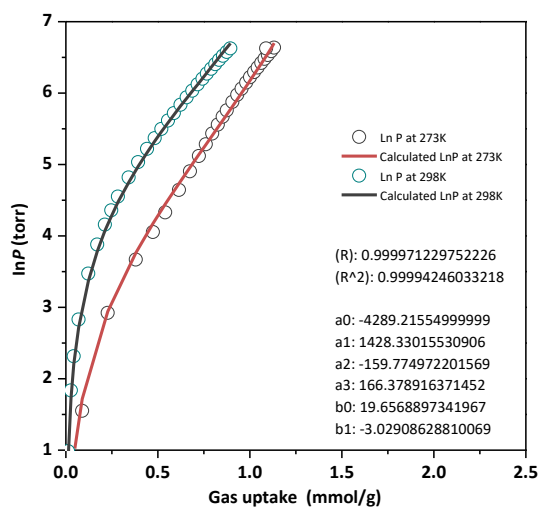


Figure S39. The calculated virial equation isotherms parameters fit to the experimental CO_2 data (at 273 and 298K) of NTU-54.

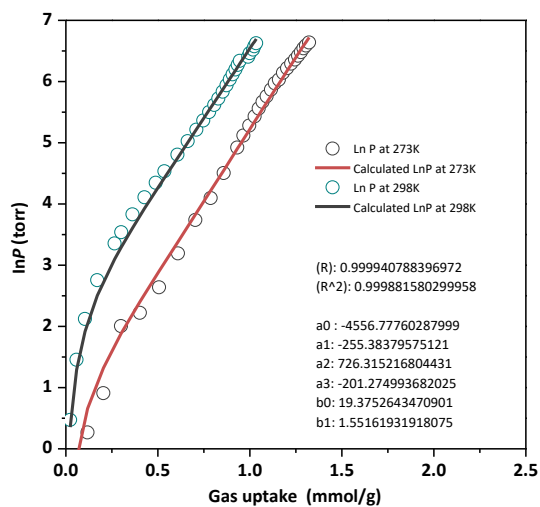


Figure S40. The calculated virial equation isotherms parameters fit to the experimental C_2H_2 data (at 273 and 298K) of NTU-54.

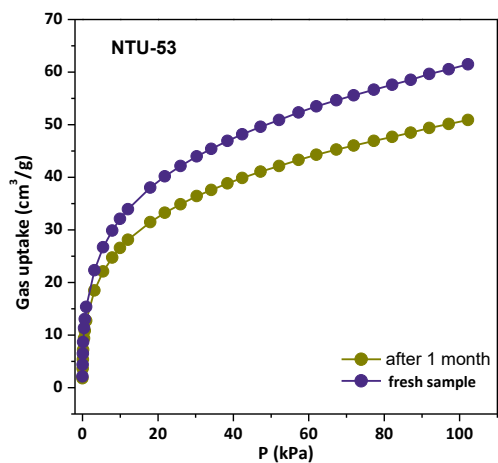


Figure S41. CO_2 adsorption and desorption isotherms of fresh sample and the sample soaked in water for 1 month of NTU-53 at 273 K.

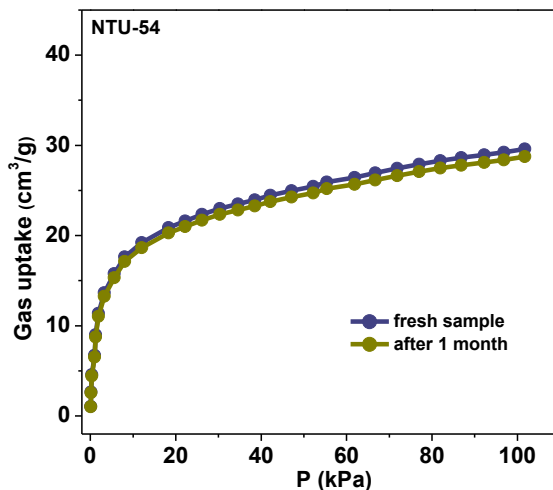


Figure S42. CO₂ adsorption and desorption isotherms of fresh sample and the sample soaked in water for 1 month of NTU-54 at 273 K.

7. Ideal selectivity calculation

Ideal adsorbed solution theory was used to predict binary mixture adsorption from the experimental pure-gas isotherms. Dual-site Langmuir-Freundlich model were used to fit the pure isotherms, where the equation is

$$q = q_{m1} \cdot \frac{b_1 \cdot P^{1/n_1}}{1 + b_1 \cdot P^{1/n_1}} + q_{m2} \cdot \frac{b_2 \cdot P^{1/n_2}}{1 + b_2 \cdot P^{1/n_2}} \quad (3)$$

Here, P is the pressure of the bulk gas at equilibrium with the adsorbed phase (kPa), q is the adsorbed amount per mass of adsorbent (mol/kg), q_{m1} and q_{m2} are the saturation capacities of sites 1 and 2 (mol/kg), b_1 and b_2 are the affinity coefficients of sites 1 (1/kPa), and n_1 and n_2 represent the deviations from an ideal homogeneous surface. The R_2 values for all the fitted isotherms were over 0.9999.

Table S2. Parameters of the ideal adsorbed solution theory of **NTU-51** to **NTU-54**.

	NTU-51		NTU-52		NTU-53		NTU-54	
	CO ₂	C ₂ H ₂						
q _{m1}	1.363567501	0.254587356	0.315597093	1792.388294	1.70798098	0.651975183	0.374889889	61.04363233
b1	0.038517875	0.276135785	0.290978662	1.00E-06	0.013396767	1.301078241	0.072197277	2.40E-03
n1	0.791043851	0.987643335	0.948421198	1.062627751	1.078955433	0.5760177	1.541789188	0.369112758
q _{m2}	0.255867663	3.118955011	0.771784382	0.673155166	1.399025881	7.863291262	14.45179599	0.525704486
b2	0.182068152	0.067986031	0.035395914	0.486031887	0.441252347	0.047651264	0.006564097	0.632720133
n2	0.957949978	0.426596837	0.802454358	0.501361701	1.00762938	0.456428108	0.462521509	1.212772209

8. References:

1. H. Wang, H. Cao, J. J. Zheng, S. Mathew, N. Hosono, B. Zhou, H. Lyu, S. Kusaka, W. Jin, S. Kitagawa and J. Duan, *Chem Eur J*, 2018, **24**, 6412-6417.
2. G. M. Sheldrick, *Acta Crystallogr. Sec. A*, 2008, **64**, 112-122.
3. A. L. Spek, *PLATON, A Multipurpose Crystallographic Tool (Utrecht University, 2001)*.
4. P. Vandersluis and A. L. Spek, *Acta Crystallogr. Sec. A*, 1990, **46**, 194-201.
5. S. S. Y. Chui, S. M. F. Lo, J. P. H. Charmant, A. G. Orpen and I. D. Williams, *Science*, 1999, **283**, 1148-1150.
6. W. J. Zhuang, S. Q. Ma, X. S. Wang, D. Q. Yuan, J. R. Li, D. Zhao and H. C. Zhou, *Chem. Commun.*, 2010, **46**, 5223-5225.
7. Y. Peng, G. Srinivas, C. E. Wilmer, I. Eryazici, R. Q. Snurr, J. T. Hupp, T. Yildirim and O. K. Farha, *Chem. Commun.*, 2013, **49**, 2992-2994.
8. R. Banerjee, A. Phan, B. Wang, C. Knobler, H. Furukawa, M. O'Keeffe and O. M. Yaghi, *Science*, 2008, **319**, 939-943.
9. D. Zhao, D. Q. Yuan, D. F. Sun and H. C. Zhou, *J. Am. Chem. Soc.*, 2009, **131**, 9186.
10. O. K. Farha, A. O. Yazaydin, I. Eryazici, C. D. Malliakas, B. G. Hauser, M. G. Kanatzidis, S. T. Nguyen, R. Q. Snurr and J. T. Hupp, *Nat. Chem.*, 2010, **2**, 944-948.
11. D. Q. Yuan, D. Zhao, D. F. Sun and H. C. Zhou, *Angew. Chem. Int. Ed.*, 2010, **49**, 5357-5361.
12. J. Duan, M. Higuchi, J. Zheng, S. I. Noro, I. Y. Chang, K. Hyeon-Deuk, S. Mathew, S. Kusaka, E. Sivaniah, R. Matsuda, S. Sakaki and S. Kitagawa, *J. Am. Chem. Soc.*, 2017, **139**, 11576-11583.
13. J. G. Duan, W. Q. Jin and R. Krishna, *Inorg. Chem.*, 2015, **54**, 4279-4284.